Analyzing the effects of void characteristics on the compliance of topology optimized structures for additive manufacturing

Brahim Benaissa[1*], Musaddiq Al Ali[1], Bochra Khatir[2], Morteza Saadatmorad[3]

[1]Toyota Technological Institute, Nagoya, Japan
[2]University Centre of Naama, Naama, Algeria
[3]Babol Noshirvani University of Technology, Babol, Iran
[*]Corresponding author: brahim.benaissa@ou.edu.vn

ARTICLE INFO

DOI:10.46223/HCMCOUJS.acs.en.15.1.66.2025

Received: August 02nd, 2024
Revised: November 25th, 2024
Accepted: December 17th, 2024

Keywords:
additive manufacturing; rejection and admission; sequential element; structural compliance; topology optimization

ABSTRACT

This study investigates the impact of void parameters, such as number, shape, and size, on the structural compliance of topology-optimized structures in additive manufacturing. The optimization uses the Sequential Element Rejection and Admission algorithm with a cantilever beam model subjected to a vertical load. Voids, modeled as elliptical regions with varying aspect ratios and saturations, are introduced into the optimized structure to simulate potential manufacturing defects. The influence of these void parameters on compliance is evaluated through finite element analysis, focusing on the relationship between void saturation, aspect ratio, and void size. The results indicate compliance increases with higher void saturations; the impact of void shape is more pronounced at high saturations. These findings provide insights into optimizing void characteristics for enhanced structural performance in additive manufacturing.

1. Introduction

Additively Manufactured (AM) Optimized Structures represent a significant advancement in engineering and manufacturing (Plocher & Panesar, 2019). A primary advantage of AM structures is the ability to produce complex geometries with lighter and stronger components, which is particularly beneficial in aerospace and automotive industries where weight reduction is crucial. Additionally, additive manufacturing facilitates rapid prototyping and production (Al Ali et al., 2024), reducing lead times and enabling iterative testing and design improvements (Al Ali et al., 2022).

However, AM Optimized Structures are reported to have issues related to AM parts' mechanical properties and reliability (Lynch et al., 2018; Zhengkai et al., 2023), as the layer-by-layer construction can introduce defects and inconsistencies. Furthermore, the scalability of additive manufacturing for mass production remains limited, often rendering it less efficient for large-scale manufacturing than conventional methods. A significant issue is the potential for voids to form within the material during the layer-by-layer deposition process. These voids can weaken the structure, reducing mechanical strength and durability. Such voids often result in inconsistencies within the material that may not be immediately visible but can affect the part's overall performance, particularly under stress or load (Smith et al., 2016).

Zhu et al. (2021) discuss the structural fatigue performance of materials produced through Additive Manufacturing (AM), particularly for aerospace applications. It highlights that AM materials, such as Selective Laser Melted (SLM) 17-4 PH stainless steel, exhibit significantly lower fatigue life and strength than their wrought counterparts due to defects like unmelted regions and gas pores. The review emphasizes the need for improved post-manufacturing treatments, such as hot isostatic pressing and surface treatments, and effective topology optimization to enhance the fatigue performance of AM parts, while also noting the challenges posed by microstructural anisotropy and the differences in thermal history between experimental samples and genuine parts.

Dana et al. (2019) investigated the impact of printing direction on tensile properties. Four printing orientations were considered: 0°, 90°, alternating 0°/90°, and alternating -45°/45°. The fracture surface analysis revealed microstructural features like layers, beads, and droplets affecting fracture modes. X-ray tomography confirmed a porosity network structured by printing paths, influencing material properties. The analysis of voids across different zones revealed macro and microvoids, illustrating cavities between layers and porosities within droplets. Cantrell et al. (2017) evaluated the anisotropic properties of 3D-printed Polycarbonate (PC) and Acrylonitrile Butadiene Styrene (ABS) specimens using various raster and build orientations.

Villarraga et al. (2015) focused on evaluating Additive Manufacturing (AM) processes through Computed Tomography (CT) scanning. AM1 had a printing resolution of approximately 100μm, which is coarser compared to the 0.5μm resolution of AM2. The research revealed varying defect densities within parts manufactured by these processes. The voids ranged mostly from 0.002mm³ to 0.2mm³ in size. This finer resolution of AM2 contributed to the reduced occurrence of voids and improved material integrity within the manufactured parts.

Research in additive manufacturing has addressed the challenge of occluded voids through various innovative methodologies. Harzheim and Graf (2006) focused on removing occluded voids by strategically eliminating material from the outside. Lu and Chen (2012) further developed this by exploring additional search directions to enhance design optimization. Eiliat and Urbanic (2018) suggested a method to minimize voids in additive manufacturing material extrusion processes through optimized tool path generation. Zhou and Zhang (2019) presented a side constraint scheme with void features to improve structural connectivity in topology optimization.

Lee et al. (2019) focused on analyzing the interlayer formation in concrete structures built using Additive Manufacturing (AM), specifically 3D printing techniques. Using Computed Tomography (CT), the study examined the correlation between porosity and tensile bond strength in the interlayers of 13 specimens. The findings revealed that the interlayers had higher porosity, and all fractures occurred along the interlayers, though no direct correlation between porosity and tensile bond strength was established.

Gaynor and Johnson (2020) suggested a projection-based topology optimization approach to eliminate occluded void geometries in additive manufacturing designs, ensuring all void regions have drainage pathways to outer surfaces. Hernandez-Contreras et al. (2020) investigate the relationship between geometric descriptors and mechanical properties in FDM components. Suggesting the descriptor $\mu(\alpha)$, representing void orientation angle, demonstrates a significant relationship between yield strength and Young's modulus in Fused Deposition Modeling (FDM) parts. $\mu(\alpha)$ indicates the direction of void growth within the internal structure of components. A closer alignment of $\mu(\alpha)$ to 0 degrees correlates with enhanced mechanical performance

Optimization algorithms have emerged as an efficient tool to solve various engineering problems (Behtani et al., 2022; Brahim et al., 2024); Benaissa et al. (2024) focused on applying topology optimization techniques to improve void tolerance in structural systems by integrating spatial analysis, YUKI algorithm. The suggested approach identifies the worst-case void scenarios in different structural shapes, boundary conditions, and sizes.

Hernandez-Contreras et al. (2020) developed void descriptors in FDM materials using global and local classifications. Global descriptors include the Void-to-volume Ratio (VR), while local descriptors cover specific void characteristics like size (1D diameter, projected size, area, and voxel count) and shape (sphericity and compactness). The CT scans and porosity analysis indicate that the void size and orientation varied across samples. Specifically, voids grew in different directions depending on the sample's orientation relative to the applied load axis. To quantify these descriptors in samples with different orientations. In the case of a typical tensile test specimen. Their data reveal no significant correlation between void characteristics and mechanical performance. However, this observation may not necessarily extend to topologically optimized structures, in which substantial voids are strategically introduced at specific locations and shapes to achieve weight reduction. Further investigation is required to determine if similar correlations hold for these optimized configurations.

This study aims to simulate voids to assess topology optimization's efficacy and investigate the impact of varying void parameters such as number, shape, and void size on structural compliance. The paper is structured as follows: the following section presents the topology optimization problem based on the SERA method. The third section describes the suggested approach to simulating Enclosed Void Generation and investigates the introduction of voids within the topology-optimized structure. The Results and Discussion section discusses the impact of varying void parameters on stiffness and deformation, providing insights into how void saturation and shape influence structural performance.

2. Topology optimization with SERA algorithm

The Cantilever beam problem is a standard benchmark in topology optimization studies, as illustrated in Figure 1. This study considers a large dimensional case of dimensions of 2,000mm in length and 1,000mm in width, subjected to a vertical downward force applied at the top of its right side. For modeling, we used bilinear structured finite element discretization with an element size of $1mm^2$.

In topology optimization, the primary objective is to identify the optimal material distribution within a predefined design domain to minimize structural deformation under specified loading conditions while adhering to a volume constraint. This optimization problem is typically formulated to reduce the structure's compliance (or maximize stiffness), ensuring it performs efficiently under applied forces. The process involves the manipulation of global displacement and force vectors, which represent the system's response to external loads, and using stiffness matrices, which define the relationship between material properties and deformation (Brackett et al., 2011).

The **Sequential Element Rejection and Admission (SERA)** approach, a method that uses discrete density variables (either 0 or 1), is beneficial for ensuring that the resulting stiffness matrix remains non-singular during the optimization process (Rozvany & Querin, 2002). To avoid issues with singularity and improve numerical stability, SERA incorporates a **non-zero lower bound** on the material density, ensuring that the densities do not become too small and that the structure remains effectively defined.

For a structural design problem aimed at maximizing stiffness, the topology optimization problem can be formulated as follows:

$$\text{Minimize } \rho \text{ such as } c(\rho)U^T KU = \sum_{e=1}^{N} U_e^T K_e U_e \quad (1)$$

Figure 1

Cantilever Beam Problem

Source. The researcher's data analysis

Where:

- U_e is the displacement vector of the e[th] element,
- K_e is the stiffness matrix of the e[th] element,
- The summation runs over all N elements in the design domain.

The topology optimization problem is subject to Volume Constraint, Element Density Bounds and the Equilibrium Equation. The objective function $c(\rho)$ represents the total stiffness of the structure, with the goal being to **maximize** this stiffness through the optimization of the material distribution ρ_e at each element level. The design variable ρ_e is constrained to take values between a lower bound, ρ_{min}, and an upper bound of 1, effectively indicating whether material is present in the element.

The total volume of material used in the structure should not exceed a prescribed fraction of the available design space:

$$\frac{V(\rho)}{V_0} = \sum_{e=1}^{N} \frac{\rho_e V_e}{V_0} \leq f\rho_e \quad (2)$$

Where:

- $V(\rho)$ is the total volume of material used in the design (based on the material densities ρ_e at each element),
- V_0 is the total available volume in the design domain,
- V_e is the volume of the e[th] element,
- f is a given fraction that limits the material usage.

The material density ρ_e for each element must lie between a lower bound ρ_{min}, set in this study as $\rho_{min} = 10^{-6}$ and an upper bound of 1:

$$\rho_{min} \leq \rho_e \leq 1 \; for \; e = 1, \dots, N \quad (3)$$

This ensures that elements are either filled with material or remain empty and prevents the density from becoming arbitrarily small, which could lead to singular stiffness matrices.

The equilibrium condition for the structure, given an applied force F, is expressed by the linear static equilibrium equation:

$$K(\rho)U = F \tag{4}$$

Where $K(\rho)$ is the global stiffness matrix, which depends on the material distribution ρ, and U is the worldwide displacement vector. The forces F are applied to the structure, and the displacements U are the unknowns to be solved for in the optimization process.

The SERA approach iteratively updates the material densities. ρ_e for each element. In this method, elements are initially assumed to have complete material (ρ_e= 1), and during the optimization process, elements may be either "rejected" (where the density ρ_e is reduced to 0) or "admitted" (where ρ_e is allowed to remain at 1 or take intermediate values above ρ_{min}) based on their contribution to the structural stiffness. By enforcing a **non-zero lower bound** on the densities, the method ensures that the stiffness matrix $K(\rho)$ remains invertible and prevents the collapse of the structure into a trivial, singular state.

The optimization is typically solved using a gradient-based or projection-based method. The sensitivities of the objective function and constraints concerning the design variables ρ_e are computed, and the material distribution is updated iteratively. This process continues until convergence is achieved, where the design variables are used. ρ_e no longer change significantly, and the optimal material layout that satisfies the stiffness maximization objective and constraints is obtained.

3. Enclosed Void simulation

Introducing damage into a topologically optimized structure conducts spatial analysis under geometric constraints. The goal is to identify valid positions within the structure where damage, represented by a void region, can be introduced without compromising the integrity of the surrounding material. This approach uses a damage radius and margin factor to determine potential locations, ensuring the damage is appropriately sized and positioned within the structural body. The damage is modeled as an elliptical void, and its placement is governed by several factors, including the damage's size and orientation (Benaissa et al., 2023).

The damage region is represented by an elliptical shape with a semi-major axis a and semi-minor axis b, where the size of the damage is defined by the ratio. $\frac{a}{b}$ and its total area. The damage is introduced to the structure by creating a binary mask that identifies the void area. This mask is used to update the structural shape matrix, replacing the corresponding elements with void values and effectively removing material from the structure in that region. The following general form of the void region describes the damage. V_d in Cartesian coordinates:

$$\frac{x^2}{a^2} + \frac{y^2}{b^2} = 1 \tag{5}$$

Where x and y are the coordinates of the points within the damaged region, and a and b are the semi-major and semi-minor axes of the elliptical void, respectively. To ensure the damage is positioned correctly, the following constraints are applied. The center of the damage must lie within the material regions of the structure. The conditions enforce this:

$$\rho(x, y) = 1 \tag{6}$$

Where $\rho(x, y)$ represents the material density at each point (x, y) in the design space, and $\rho = 1$ corresponds to an excellent region of the structure.

The margin factor δ is introduced to account for a slight overlap between the edge of the void and the material boundary. This allows the interaction between the damaged region and the material edge to be set. The user can enable the damage to overlap or exceed the material edge or set up a simulation where all damages are internal, which is considered in this study (Benaissa et al., 2023). The margin can be mathematically expressed as:

$$\left|\frac{\partial \rho}{\partial x}\right| \leq \delta \text{ and } \left|\frac{\partial \rho}{\partial y}\right| \leq \delta \tag{7}$$

Figure 2

Illustration of Void Aspect Ratio Variations with Exaggerated Void Sizes

Source. The researcher's data analysis

The maximum number of valid void positions depends on the available material area, the void size, and the margin enforced to avoid overlap. The number of valid damage positions is calculated by discretizing the structural domain and counting the elliptical voids, considering the margin. To calculate this, we first define the available material area. $A_{material}$, which is the total area of the structure that contains material ($\rho = 1$). Next, define the location of a single damaged region, A_{void}, which is the area of the elliptical void defined by the semi-major axis a and semi-minor axis b. Taking into account the margin, set as a percent of the total damage area.

$$A_{void} = \pi \cdot a \cdot b \cdot (1 + \delta) \tag{8}$$

The maximum number of void positions N_{max} can be calculated by dividing the material area by the area of a single void region:

$$N_{max} = \left|\frac{A_{material}}{A_{void}}\right| \tag{9}$$

This calculation helps assess the impact of voids on overall structural performance, simulating voids that may occur during the additive manufacturing process. The number of voids is determined based on the quality of the manufacturing technique relative to the maximum possible number of voids. In this study, we consider different levels of void quantity. Figure 2 and Figure 3 illustrate the variation of void aspect ratio and size and quantity, respectively. This study sets the size as a ratio between the void size and the structure volume.

To evaluate the structural response to the introduced voids, FEA is performed to compute the stiffness matrix $K(\rho_v)$ and displacement vector U of the structure with the applied voids under specific boundary conditions. The structural compliance is calculated as:

$$f(\rho_v) = U^T K(\rho_v) U \tag{10}$$

Figure 3

Illustration of the Case of Void Sizes Examined in this Study

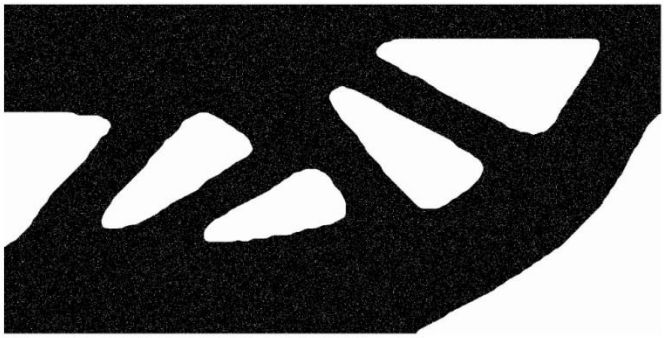

Source. The researcher's data analysis

Where $K(\rho_d)$ is the stiffness matrix modified by the voids, and U is the displacement vector that results from the applied load.

4. Results and discussions

This study investigates the impact of varying void parameters, such as number, shape, and void size, on structural compliance in topologically optimized structures. The experiment tests the compliance of materials with varying Aspect Ratios (AR) and Void Saturations (VS) at different void sizes.

Figure 4

Compliance Response Surface for Varying Aspect Ratios and Void Saturations at a Void Size of 0.001

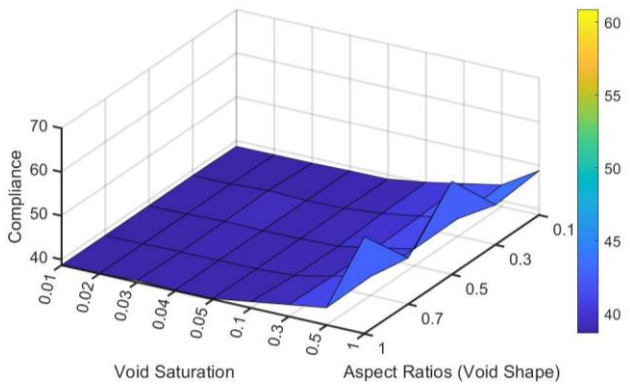

Source. Data analysis result of the research

Figure 5

Compliance Response Surface for Varying Aspect Ratios and Void Saturations at a Void Size of 0.0005

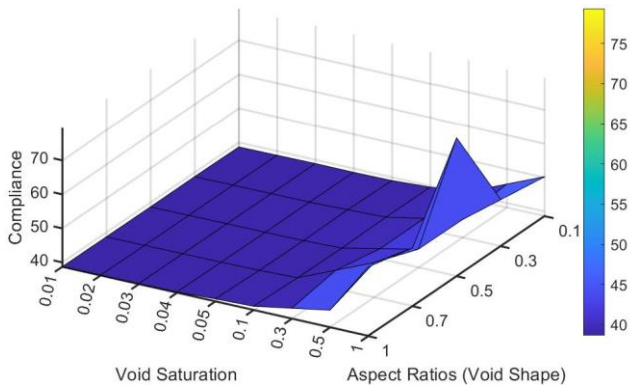

Source. Data analysis result of the research

Figure 6

Compliance Response Surface for Varying Aspect Ratios and Void Saturations at a Void Size of 0.0001

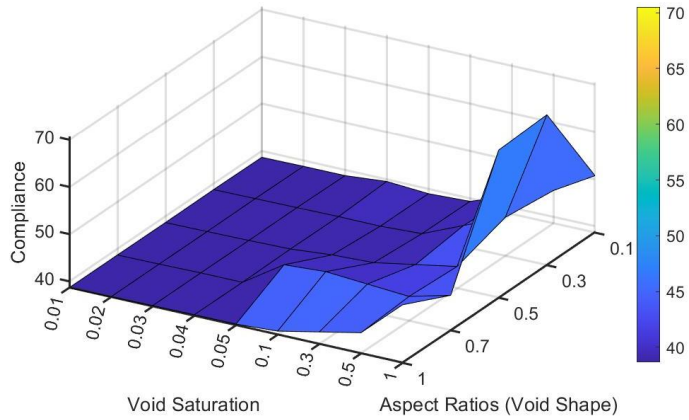

Source. Data analysis result of the research

Figure 7

Compliance Response Surface for Varying Aspect Ratios and Void Saturations at a Void Size of 0.00005

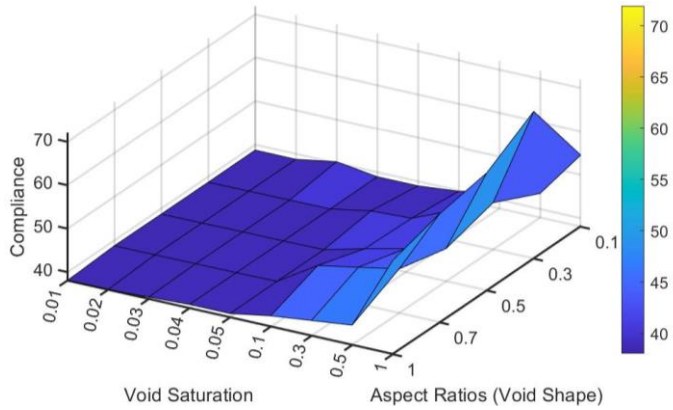

Source. Data analysis result of the research

The aspect ratios range from 0.1 (sharp elliptical voids) to 1 (circular voids). In contrast, void saturations vary from 1% to 100%, representing the number of existing voids in the structure compared to the maximum number of possible voids according to the selected parameters of void size, structure size, and the margin of overlap. The void volume ratio defines void size compared to total structural volume; the considered cases include the four ratios: 0.001, 0.0001, 0.0005, and 0.00005.

Compliance values (N·m) for each combination are shown in four figures. Each figure presents a compliance response surface for varying aspect ratios and void saturations at void sizes of 0.001, 0.0005, 0.0001, and 0.00005. defined as the ratio between void volume and structural volume. These figures illustrate how the material's compliance changes with these void parameters.

4.1. Influence of enclosed void saturation

Void saturation, representing the percentage of voids in the structure, directly correlates with compliance: At low void saturations (1% to 5%), compliance values are relatively low and stable across different void sizes and aspect ratios. This indicates that small amounts of voids have minimal impact on structural rigidity and deformation. The material retains most of its original stiffness, showing minimal changes in compliance.

Compliance shows more variability as void saturation increases (10% to 30%). Medium levels of void saturation lead to moderate increases in compliance, particularly noticeable in structures with medium to large void sizes. This suggests that as voids become more prevalent, the material's stiffness decreases, leading to increased deformation.

High void saturations (50% to 100%) have the highest compliance values. Structures with a high percentage of voids exhibit significant increases in deformation under load. This effect is pronounced in materials with larger void sizes and higher aspect ratios. High void saturation dramatically reduces structural integrity, making the material much more compliant and prone to bending or collapsing under applied stresses.

4.2. Influence of enclosed void shape

The study analyzes the impact of void shape, indicated by Aspect Ratio (AR), on the compliance of topologically optimized structures across various void size ratios. The aspect ratios range from 0.1 (sharp elliptical voids) to 1 (circular voids), highlighting the influence of void shape on material performance.

At large Void Size, the compliance values remain relatively stable across aspect ratios at small Void Saturations (0.01 - 0.05) with minimal differences. However, Compliance increases across all aspect ratios at High Void Saturations (0.1 - 1), with circular voids exhibiting slightly higher compliance values than elliptical voids.

At Medium Void Size: 0.0001 - 0.0005, the compliance is nearly uniform across different aspect ratios, showing negligible impact of void shape. Compliance increases noticeably, with circular voids showing higher compliance values, indicating a more significant effect of void shape at higher saturations.

Figure 8

Compliance Response Surface for Varying Enclosed Void Shape

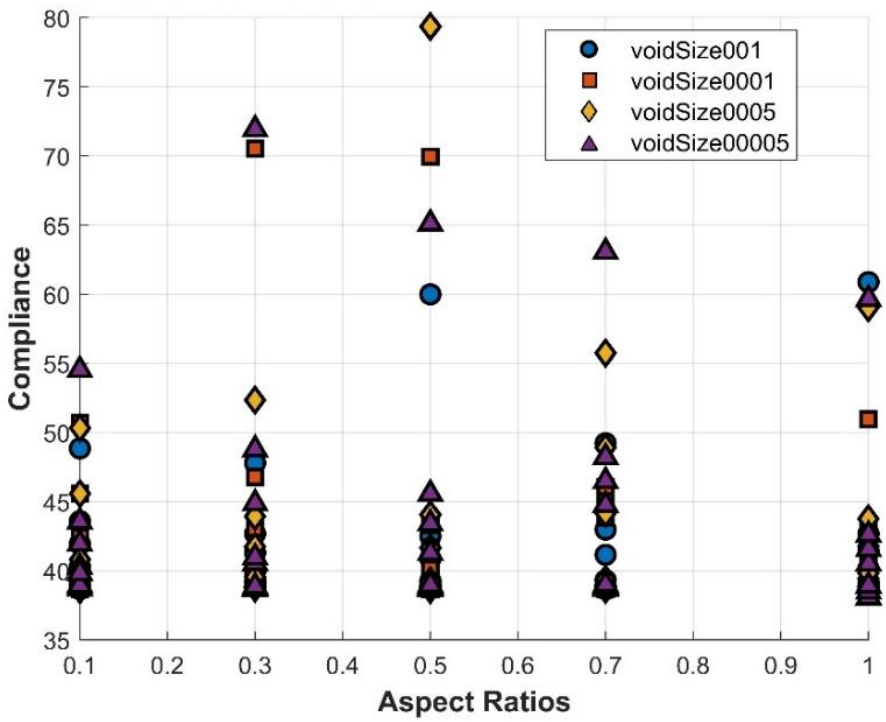

Source. Data analysis result of the research

At a small Void Size of 0.00005, Compliance values are relatively similar across different aspect ratios. However, at High Void Saturations (0.1 - 1), the compliance values increase, with circular voids consistently showing higher compliance than elliptical voids, reinforcing the pattern observed in other void size ratios.

Across all void size ratios, the study demonstrates that compliance values are relatively stable at low void saturations but increase at higher saturations, generally exhibiting higher compliance with elliptical voids, except for sizeable void case, where the circular void has the same effect, possibly due to significant collective void volume, highlighting the moderate impact of void shape on structural compliance. The following figure provides a comparison of how varying void sizes and aspect ratios influence structural compliance.

5. Conclusions

The studies on the influence of void characteristics on the mechanical performance of topology-optimized structures in additive manufacturing reveal essential insights into the relationship between void saturation, size, shape, and structural compliance. The observations suggest increased void saturation generally leads to greater compliance, particularly when saturation exceeds 50%. Furthermore, void size and shape are critical factors, with circular voids showing higher compliance than elliptical voids at higher saturations. The findings suggest that void shape has a minimal effect at smaller and medium void sizes but becomes more significant at higher and smaller ones. These results underscore the importance of considering void parameters in optimizing the mechanical performance of additively manufactured components.

References

Al Ali, M., Shimoda, M., Benaissa, B., & Kobayashi, M. (2022). *Concurrent multiscale hybrid topology optimization for light weight porous soft robotic hand with high cellular stiffness* [Paper presentation]. International Conference of Steel and Composite for Engineering Structures, Lecce, Italy.

Al Ali, M., Shimoda, M., Benaissa, B., Kobayashi, M., Takeuchi, T., Al-Shawk, A., & Ranjbar, S. (2024). Metaheuristic aided structural topology optimization method for heat sink design with low electromagnetic interference. *Scientific Reports, 14*(1), Aticle 3431.

Behtani, A., Tiachacht, S., Khatir, T., Khatir, S., Wahab, M. A., & Benaissa, B. (2022). Residual force method for damage identification in a laminated composite plate with different boundary conditions. *Frattura ed Integrità Strutturale, 16*(59), 35-48.

Benaissa, B., Al Ali, M., Kobayashi, M., Le, C. T., & Khatir, S. (2023). *Damage tolerance in topologically optimized structures: Exploring structural integrity through worst-case damage optimization* [Paper presentation]. International Conference of Steel and Composite for Engineering Structures, Lecce, Italy.

Benaissa, B., Kobayashi, M., Al Ali, M., Khatir, S., & Shimoda, M. (2024). A novel exploration strategy for the YUKI algorithm for topology optimization with metaheuristic structural binary distribution. *Engineering Optimization*, 1-21.

Brackett, D., Ashcroft, I., & Hague, R. (2011). *Topology optimization for additive manufacturing.* https://utw10945.utweb.utexas.edu/Manuscripts/2011/2011-27-Brackett.pdf

Brahim, B., Kobayashi, M., Al Ali, M., Khatir, T., & Elmeliani, M. E. A. E. (2024). Metaheuristic optimization algorithms: An overview. *HCMCOU Journal of Science-Advances in Computational Structures, 14*(1), 34-62.

Cantrell, J. T., Rohde, S., Damiani, D., Gurnani, R., DiSandro, L., Anton, J., Young, A., Jerez, A., Steinbach, D., Kroese, C., & Ifju, P. (2017). Experimental characterization of the mechanical properties of 3D-printed ABS and polycarbonate parts. *Rapid Prototyping Journal, 23*(4), 811-824.

Dana, H. R., Barbe, F., Delbreilh, L., Azzouna, M. B., Guillet, A., & Breteau, T. (2019). Polymer additive manufacturing of ABS structure: Influence of printing direction on mechanical properties. *Journal of Manufacturing Processes, 44*, 288-298.

Eiliat, H., & Urbanic, J. (2018). Visualizing, analyzing, and managing voids in the material extrusion process. *The International Journal of Advanced Manufacturing Technology, 96*, 4095-4109.

Gaynor, A. T., & Johnson, T. E. (2020). Eliminating occluded voids in additive manufacturing design via a projection-based topology optimization scheme. *Additive Manufacturing, 33*, Article 101149.

Harzheim, L., & Graf, G. (2006). A review of optimization of cast parts using topology optimization: II-Topology optimization with manufacturing constraints. *Structural and Multidisciplinary Optimization, 31*, 388-399.

Hernandez-Contreras, A., Ruiz-Huerta, L., Caballero-Ruiz, A., Moock, V., & Siller, H. R. (2020). Extended CT void analysis in FDM additive manufacturing components. *Materials, 13*(17), Article 3831.

Lee, H., Kim, J. H. J., Moon, J. H., Kim, W. W., & Seo, E. A. (2019). Correlation between pore characteristics and tensile bond strength of additive manufactured mortar using X-ray computed tomography. *Construction and Building Materials, 226*, 712-720.

Lu, J., & Chen, Y. (2012). Manufacturable mechanical part design with constrained topology optimization. *Proceedings of the Institution of Mechanical Engineers, Part B: Journal of Engineering Manufacture, 226*(10), 1727-1735.

Lynch, M. E., Mordasky, M., Cheng, L., & To, A. (2018). Design, testing, and mechanical behavior of additively manufactured casing with optimized lattice structure. *Additive Manufacturing, 22*, 462-471.

Plocher, J., & Panesar, A. (2019). Review on design and structural optimisation in additive manufacturing: Towards next-generation lightweight structures. *Materials & Design, 183*, Article 108164.

Rozvany, G., & Querin, O. (2002). *Theoretical foundations of Sequential Element Rejections and Admissions (SERA) methods and their computational implementation in topology optimization* [Paper presentation]. 9th AIAA/ISSMO Symposium on Multidisciplinary Analysis and Optimization, Washington, USA .

Smith, C. J., Gilbert, M., Todd, I., & Derguti, F. (2016). Application of layout optimization to the design of additively manufactured metallic components. *Structural and Multidisciplinary Optimization, 54*, 1297-1313.

Villarraga, H., Lee, C., Corbett, T., Tarbutton, J. A., & Smith, S. T. (2015). *Assessing additive manufacturing processes with X-ray CT metrology* [Paper presentation]. ASPE Spring Topical Meeting: Achieving Precision Tolerances in Additive Manufacturing, Raleigh, USA.

Zhengkai, W., Wu, S., Qian, W., Zhang, H., Zhu, H., Chen, Q., Zhang, Z. X., Guo, F., Wang, J., & Withers, P. J. (2023). Structural integrity issues of additively manufactured railway components: Progress and challenges. *Engineering Failure Analysis, 149*, Article 107265.

Zhou, L., & Zhang, W. (2019). Topology optimization method with elimination of enclosed voids. *Structural and Multidisciplinary Optimization, 60*, 117-136.

Zhu, Z., Zhou, H., Wang, C., Zhou, L., Yuan, S., & Zhang, W. (2021). A review of topology optimization for additive manufacturing: Status and challenges. *Chinese Journal of Aeronautics, 34*(1), 91-110.